Horizontal Motion of a Superhydrophobic Substrate Affects the Drop Bouncing Dynamics

Haiyang Zhan,[1] Chenguang Lu,[1] Cong Liu,[1] Zuankai Wang,[2] Cunjing Lv,[3,*] and Yahua Liu[1,†]
[1]Key Laboratory for Precision and Non-Traditional Machining Technology of Ministry of Education, Dalian University of Technology, Dalian 116024, China
[2]Department of Mechanical Engineering, City University of Hong Kong, Hong Kong 999077, China
[3]Department of Engineering Mechanics, Tsinghua University, Beijing 100084, China

(Received 21 October 2020; revised 10 February 2021; accepted 11 May 2021; published 11 June 2021)

While the drop impact dynamics on stationary surfaces has been widely studied, the way a drop impacts a moving solid is by far less known. Here, we report the physical mechanisms of water drops impacting on superhydrophobic surfaces with horizontal motions. We find that a viscous force is created due to the entrainment of a thin air layer between the liquid and solid interfaces, which competes with the capillary and inertia forces, leading to an asymmetric elongation of the drop and an unexpected contact time reduction. Our experimental and theoretical results uncover consolidated scaling relations: the maximum spreading diameter is controlled by both the Weber and capillary numbers $D_{\max}/D_0 \sim \mathrm{We}^{1/4}\mathrm{Ca}^{1/6}$, while the dimensionless contact time depends on the capillary number $\tau/\tau_0 \sim \mathrm{Ca}^{-1/6}$. These findings strengthen our fundamental understandings of interactions between drops and moving solids and open up new opportunities for controlling the preferred water repellency through largely unexplored active approaches.

DOI: 10.1103/PhysRevLett.126.234503

One of the most landmark properties of water repellant surfaces is that the impacting droplet can bounce off easily, either going through a typical spreading and retraction stage or exhibiting a pancake shape [1–3]. The impinging drop usually manifests a remarkable elasticity because of the negligible viscous dissipation caused by the hydrophobic roughness trapped underlying the impinging drop, which is directly related to various potential applications [4–11]. Note that the drop retains a symmetric shape during the whole impinging process. The contact time τ_0, defined as the period from the moment the drop first contacts the surface to its complete detachment, is reported to be independent of the impact velocity and depends on the inertia-capillary time scaled as $\tau_0 \sim (\rho\Omega_0/\gamma)^{1/2}$, where ρ, Ω_0, and γ are the mass density of the liquid, drop volume, and liquid-vapor surface tension, respectively [1]. This contact time is different from that on hot plates explored by Lee *et al.* [12] who distinguished the actual contact time from the time until the drop lifts off from the substrate. For the contact time controls the extent to which mass, momentum, and energy are exchanged between the drop and the substrate; and thus, contact time minimization is highly desirable in practical settings [6,7,13].

Remarkably, several attempts have been made to rectify the drop impact dynamics to lower the solid-liquid interaction on stationary surfaces, including asymmetric bouncing, pancake bouncing, and so on [2,3,13–16]. Here, we consider the situation of drops impinging on a surface with horizontal motion, on which the drop exhibits an asymmetrical bouncing process and a remarkably reduced contact time. This scenario with active regulation of drop rebounding dynamics is omnipresent in nature and emerging technological entities, such as anti-icing on high-speed flying aircraft and spinning wind turbine blades [17,18], rather than its stationary counterpart. Although drop impacting phenomena on moving hydrophilic and hydrophobic substrates have been reported very recently [18–21], in this Letter, we devote attention to revealing the underlying physics accounting for three fundamental questions: how the impact velocity and the substrate velocity affect the contact time, contact region, and horizontal displacement of the drop.

We consider a water drop impinging on a rotating superhydrophobic aluminum disk [Fig. 1(a)]. As shown in the scanning electron microscopic (SEM) image in Fig. 1(b), the surface is covered by steps and pits built up by millions of facets of a few microns and with an apparent water contact angle over 165° [Fig. 1(b), inset]. Details of the surface preparation and experimental procedure are shown in the Supplemental Material [22]. The disk is entrained by a stepper motor. The angular velocity ω

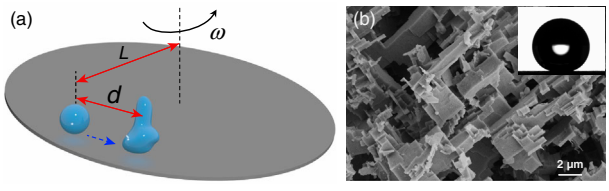

FIG. 1. (a) Schematic of the experimental setup. A water drop is deposited on a disk rotating at an angular velocity ω. (b) SEM image of the surface.

ranges from 0 to 180 rad/s, corresponding to a horizontal velocity $V = L\omega$ ranging from 0 to 3.6 m/s, where $L = 2$ cm is the distance from the impact point to the disk center. The drop dynamic behavior is simultaneously filmed from side and top views using two synchronous high-speed cameras.

Figure 2(a) shows the side and top views of a water drop with diameter $D_0 = 3.0$ mm impinging on a stationary superhydrophobic surface at $U = 0.89$ m/s, corresponding to We $= 32.9$, where $\mathrm{We} = \rho U^2 D_0/\gamma$ is defined as the Weber number with $\rho = 998$ kg/m^3 and $\gamma \approx 0.073$ N/m. The drop retains a circular symmetry during the bouncing process, and the contact time is 18.1 ms (Movie S1, right column [22]).

However, on the moving surface, as shown in Fig. 2(b), the drop exhibits a distinctively different bouncing dynamics, as exemplified by an impact at We $= 32.9$ and $V = 1.41$ m/s. A first striking observation is the asymmetrical spreading of the drop over the surface, resulting in an elongated and asymmetric outline (Movie S1, left column and Movie S2 [22]). The drop expands in all directions at the very initial stage ($t < 2$ ms) and then ($t \approx 4.1$ ms) the lamella tail (left) stops expanding, but the lamella front (right) continues to stretch along with the surface movement. Such movement keeps the lamella's front far from the bulk of the liquid where it starts to dewet from the surface at the earliest moment. After the recoiling of the drop, it entirely takes off at $\tau = 13.7$ ms, which is ~25% shorter than that on stationary surfaces. Note that, in particular, the drop bounces off and is translated horizontally with a displacement d between the impact point and the point where the drop rebounds away from the surface [Fig. 2(b)]. An increase of V results in a more prominent asymmetrical spreading of the drop and a larger lamella front, which is always the first to bounce (Fig. S1 and Movie S3 [22]).

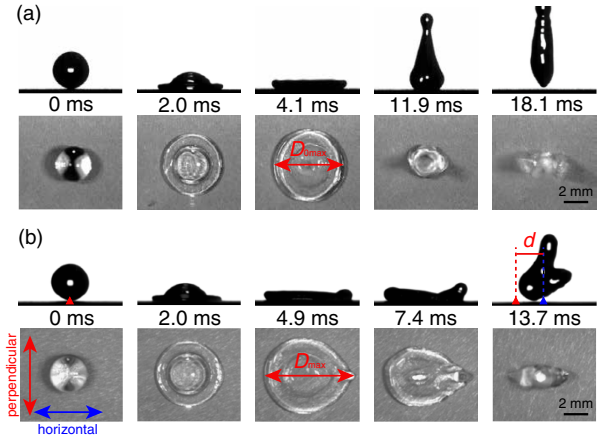

FIG. 2. (a) Selected snapshots showing a drop impinging on a stationary superhydrophobic surface (We $= 32.9$). The drop detaches from the surface at 18.1 ms. (b) Selected snapshots showing a drop impinging on a moving superhydrophobic surface at $V = 1.41$ m/s (We $= 32.9$). The drop bounces off at 13.7 ms with a horizontal displacement d.

Figure 3(a) shows the time evolution of the spreading length, defined as the width of the drop in a certain direction, on the moving surface with $V = 1.41$ m/s and a stationary surface, respectively, under We $= 32.9$. It is apparent that an impinging drop experienced an asymmetric spreading and retraction on the moving surface. Specifically, the maximum spreading length of the drop in the direction perpendicular to the surface motion (blue hollow circles) at 4.1 ms is 6.3 mm, which is close to its symmetric stationary counterpart (black squares), however, the liquid in the horizontal direction (red solid dots) continues to spread. Once the fluid in the direction perpendicular to the surface motion completes its retraction [Fig. 2(b)], the drop detaches from the surface in a deformed shape at ~13.7 ms.

Figure 3(b) shows the variation of the contact time τ as a function of V under various We, where τ decreases with V but has a weak dependence on We. This behavior is replotted in Fig. 3(c) (a normalized plot of Fig. S2 [22]), which is consistent with the classic result on stationary surfaces that τ_0 is independent of We [1]. Figures 3(b) and 3(c) suggest that the contact time is mainly modulated by the surface moving velocity. To further elucidate the dependence of the contact time τ on the surface velocity, we decompose it into the spreading time τ_s and retraction time τ_r, as shown in Fig. 3(d). It is apparent that the spreading time does not depend on V, in agreement with previous observation that the spreading is mainly dominated by the inertia [23,24]. However, the retraction time strikingly

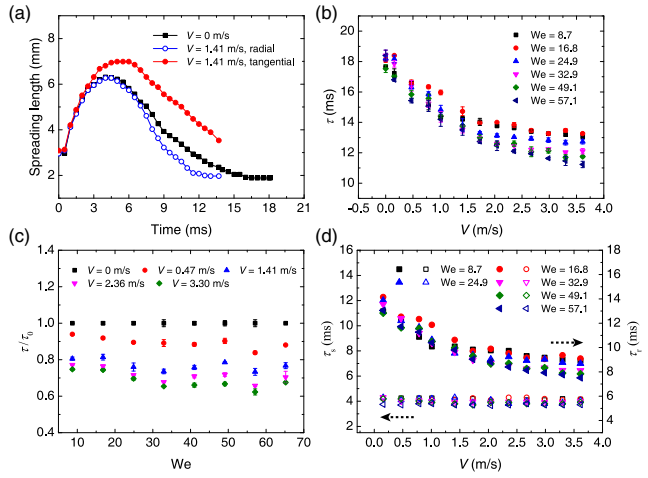

FIG. 3. (a) Spreading length over time in the directions perpendicular and parallel to the surface motion at $V = 1.41$ m/s under We $= 32.9$. The drop spreading length under the same We on the stationary surface is presented for comparison. (b) Variation of the contact time τ as a function of V. (c) Variation of the normalized contact time τ/τ_0 as a function of We. (d) Variation of the spreading time τ_s (hollow dots) and retraction time τ_r (solid dots) with V.

decreases with the surface velocity: for $V = 1.41$ m/s and $\mathrm{We} = 32.9$, the decrease in τ_r compared with the stationary surface is ~40%.

To elucidate how the moving surface reduces the contact time, first, we consider the deformation of the drop in the spreading process. When a drop impacts a stationary surface, it first spreads to its maximum diameter $D_{0\max}$ [Fig. 2(a)] with a corresponding thickness h_0 [Fig. S3(a) [22]]. $D_{0\max}$ and h_0 have been quantified on the basis of a momentum conservation [24,25]: the reinforced acceleration $a \sim U^2/D_0$ exerted on the drop during the impingement leads to $h_0 \sim [\gamma/(\rho a)]^{1/2} \sim D_0 \mathrm{We}^{-1/2}$, thus, a scaling relation $D_{0\max}/D_0 \sim \mathrm{We}^{1/4}$ is obtained [25], considering the volume conservation of the liquid $D_{0\max}^2 h_0 \sim D_0^3 \sim \Omega_0$. This scaling relation $D_{0\max}/D_0 \sim \mathrm{We}^{1/4}$ is well reproduced for a substantial range of Weber numbers in our experiments [Fig. S3(b) [22]]. However, on the moving surface, as shown in Fig. 2(b), the drop is elongated in the horizontal direction, and the characteristic maximum diameter becomes $D_{\max}$ ($D_{\max} > D_{0\max}$) with a corresponding characteristic thickness h ($h < h_0$) [Fig. S4(a) [22]]. Note that, during the impingement on the moving surface, the lamella's front always detaches [e.g., $t = 7.4$ ms in Fig. 2(b)] prior to the detachment of its tail. Considering the earlier detachment of the liquid on the lamella's front results in a reduction of the contact volume of the impinging drop, we define the remaining contact volume as Ω ($\Omega < \Omega_0$). Since the maximum spreading length of the drop along the direction perpendicular to the surface motion approximates to $D_{0\max}$, as verified by Fig. S5 [22], we have $\Omega \sim D_{0\max}^2 h$. The volume conservation $\Omega_0 \sim D_{0\max}^2 h_0 \sim D_{\max}^2 h$ leads to $\Omega \sim \Omega_0 (D_{0\max}/D_{\max})^2$. Further defining a contact time $\tau \sim (\rho\Omega/\gamma)^{1/2}$ for a drop impinging on the moving surface, we have

$$\frac{\tau}{\tau_0} \sim \sqrt{\frac{\Omega}{\Omega_0}} \sim \frac{D_{0\max}}{D_{\max}}. \tag{1}$$

Indeed, this is observed in Fig. 4(a), where the experimental data is in good agreement with Eq. (1). Note that this simple idea of reduced contact volume has been widely applied in explaining the contact time reduction with great success even for more complex cases, such as substrates with veins and singularities [3,13,26]. Furthermore, a combination of Eq. (1) and $D_{0\max}/D_0 \sim \mathrm{We}^{1/4}$ leads to

$$\frac{D_{\max}}{D_0} \sim \frac{\tau_0}{\tau} \mathrm{We}^{1/4}, \tag{2}$$

which is very well confirmed by Fig. 4(b) over a large range of the explored surface velocity V and, in turn, supports the rationality of Eq. (1). The coefficient of Eq. (2) deduced from the fit in Fig. 4(b) is 0.77 ± 0.03, which is quite close to unity.

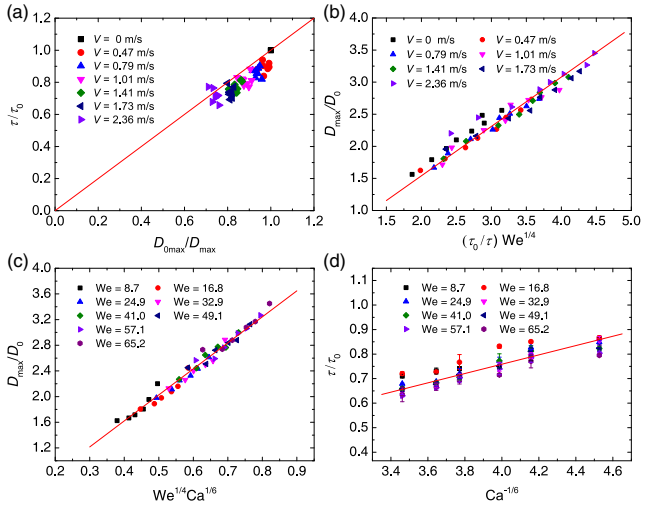

FIG. 4. (a) Normalized contact time τ/τ_0 as a function of $D_{0\max}/D_{\max}$. The dots with different colors represent different V ranging from 0 to 2.36 m/s and different U ranging from 0.46 to 1.26 m/s, corresponding to $8.7 < \mathrm{We} < 65.2$. The red line having a slope 1. (b) Replot of the data in (a) showing normalized drop diameter $D_{\max}/D_0$ as a function of $(\tau_0/\tau)\mathrm{We}^{1/4}$. (c), (d) Relationships between $D_{\max}/D_0$ and $\mathrm{We}^{1/4}\mathrm{Ca}^{1/6}$, and τ/τ_0 and $\mathrm{Ca}^{-1/6}$. The solid lines in (c) and (d) are the best fits based on Eqs. (3) and (4), respectively.

To further decouple the interplay between the contact time τ and the maximum diameter $D_{\max}$, we uncover the underlying mechanism along the following line of thought. Previous studies have indicated that the elongated drop along the moving direction of the disk is characteristic of viscous deformation [27]: during the impingement, the drop is moving on a film of air trapped between the solid and liquid interfaces, generating a kind of dynamic Leidenfrost-like phenomenon and large slip [28]. Particularly, the large static contact angle of the superhydrophobic surface favors air entrainment. The thickness of the air film is a result of a balance between viscous effects and capillarity and obeys the classical Landau-Levich-Derjaguin (LLD) law $\delta \sim l_c(\eta_a V/\gamma)^{2/3} \sim l_c \mathrm{Ca}^{2/3}$ for the case of a big drop moving on the superhydrophobic surface under its own gravity [29]. Here, $l_c = [\gamma/(\rho g)]^{1/2} \approx 2.73$ mm is defined as the capillary length for water, in which $g = 9.81$ m/s^2 is the gravity acceleration. $\mathrm{Ca} = \eta_a V/\gamma$ is defined as the capillary number (Ca), with η_a being the viscosity of air. Considering the reinforced acceleration exerted on the impinging drop, the LLD law becomes $\delta \sim h_0 \mathrm{Ca}^{2/3}$. Regarding $\eta_a \approx 18 \times 10^{-6}$ Pa s and Ca in our experiments is typically of the order of 10^{-3}, the thickness of the air film δ is calculated in the order of 1 μm, which is comparable to the texture height of the superhydrophobic surface [27].

The viscous air between the mobile drop and the moving surface exerts a drag force on the liquid, which can be approximated as $T_v D_{\max}^2 \sim \eta_a (V/\delta) D_{\max}^2$, where T_v is the

viscous shear stress of the air flow [30]. The drag force is then balanced by capillarity, scaling as $(\gamma/h)D_{\max}^2$. Hence, the force balance becomes $\eta_a V/\delta \sim \gamma/h$. A substitution of $\delta \sim h_0 \mathrm{Ca}^{2/3}$, $h_0 \sim D_0 \mathrm{We}^{-1/2}$, and $D_0^3 \sim D_{\max}^2 h$ into $\eta_a V/\delta \sim \gamma/h$ leads to

$$\frac{D_{\max}}{D_0} \sim \mathrm{We}^{1/4}\mathrm{Ca}^{1/6}. \tag{3}$$

As shown in Fig. S4(b) [22], the maximum diameter $D_{\max}$, indeed, increases with both the impact velocity U and tangential velocity V. A combination of Eqs. (2) and (3) leads to

$$\frac{\tau}{\tau_0} \sim \mathrm{Ca}^{-1/6}. \tag{4}$$

Equations (3) and (4) suggest that the maximum spreading diameter $D_{\max}$ of the impinging drop is controlled by both the Weber and capillary numbers, whereas the contact time τ is controlled by the surface velocity, which are well confirmed by the data in Figs. 4(c) and 4(d). The coefficients of Eqs. (3) and (4) deduced from the fits in Figs. 4(c) and 4(d) are 4.05 and 0.19, respectively. Moreover, Eq. (4) and Fig. 4(d) surprisingly reveal that the independency of the contact time on the impact velocity U [1] is also applicable for a drop impinging on moving surfaces. Equation (4) is further verified by a drop impacting on moving surfaces with different drop sizes, as shown in Fig. S6 [22]. Further increases of We and Ca will lead to the drop splash [24,31,32], and an analysis of this complex scenario is beyond the scope of current research [20].

Finally, we explore the horizontal displacement d of the drop translated by the surface motion [Fig. 2(b)]. In fact, three different forces exert on the drop which could be responsible for the propulsive movement in the translational direction. First, one might naturally hypothesize a Stokes force $F_S \sim \eta_a D_0 V$ due to the motion of the drop in the air. However, such a force is typically 10^{-2} μN for the millimeter-size drop in air flowing at $V = 1$ m/s. Second, considering the rotation of the disk, the interaction between the drop and the boundary layer of the air is crucial for the translating of the drop [33,34]. In this case, Reynolds number, expressed as $\mathrm{Re} = \rho_a D_0 V/\eta_a$ is of the order of 10^2 for the millimeter-size drop and $V = 1$ m/s, with the mass density of air $\rho_a = 1.293$ kg/m^3. At such a high value of Re, an inertial force F_a is expected to exert on the drop, which is characterized as $F_a \sim \rho_a V^2 D_0 \Delta \sim (\rho_a \eta_a L)^{1/2} D_0 V^{3/2}$. Here, $\Delta \approx 2.5[\eta_a L/(\rho_a V)]^{1/2}$ denotes the laminar boundary layer of air resulting from the rotation of the disk. Regarding the horizontal velocity (0.46 m/s $< V <$ 2.36 m/s) of the contact point, Δ ranges from 0.86 to 1.95 mm ($< D_0$). Consequently, F_a is estimated to be a few μN. Last, since air is sheared under the drop, i.e., δ is a few μm as aforementioned, the Reynolds number accounting for air motion in the gap of thickness δ is $\mathrm{Re} = \rho_a V \delta^2/(\eta_a D_0)$ and is estimated of the order 10^{-3} for $D_0 = 3$ mm and $V = 1$ m/s. Thus, a viscous drag F_v arising from the air moving beneath the drop scales as $F_v \sim (\eta_a V/\delta) D_{\max}^2$ (with $\eta_a V/\delta$ being the viscous stress) is exerted over the surface area $D_{\max}^2$ of the base of the impinging drop. Here, F_v is estimated to be of the order of 100 μN. Compared with F_a and F_v, F_S can be negligible. Then the force F acting on the impinging drop could be expressed as a combination of F_a and F_v, i.e., $F \approx \alpha(\eta_a V/\delta) D_{\max}^2 + \beta(\rho_a \eta_a L)^{1/2} D_0 V^{3/2}$, where α and β are numerical coefficients. Hence, the translational displacement d of the drop during the impingement could be deduced through $d \sim [F/(\rho \Omega_0)]\tau^2$, which is rewritten in dimensionless form as follows:

$$\begin{aligned}\frac{d}{D_0} &\approx \alpha \mathrm{WeCa}^{1/3} + \beta\left(\frac{\rho_a L\gamma}{\eta_a^2}\right)^{1/2}\mathrm{Ca}^{7/6} \\ &= \alpha \mathrm{WeCa}^{1/3} + \beta \mathrm{Oh}^{-1}\mathrm{Ca}^{7/6},\end{aligned} \tag{5}$$

where $\mathrm{Oh} = \eta_a/(\rho_a L\gamma)^{1/2}$ is defined as the Ohnesorge number, which relates the viscous to inertial forces of the air and the surface tension force of water, and it is a constant coefficient in our experiments. As shown in Fig. 5, the lateral distance estimated by Eq. (5) is well consistent with the experimental data, with $\alpha = 0.18$ and $\beta = 1.61$ being the best fits of the coefficients.

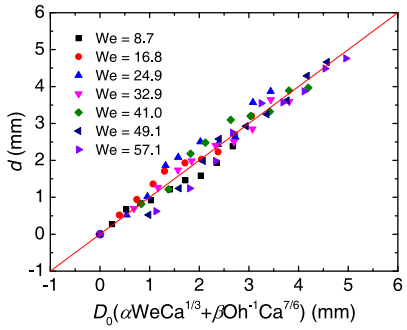

FIG. 5. Horizontal displacement d as a function of We and Ca. The solid line is the best fitting of Eq. (5).

In this Letter, we have experimentally and theoretically explored the physical mechanisms of drop impingement on moving superhydrophobic surfaces.We have shown, here, for the first time, that the dynamic behaviors such as the reduced contact time, the elongation, and horizontal distance of the drop can be generalized by simple scaling relations. The quantitative comparisons with a variety of experiments suggest that these scaling relations have successfully captured the competition between the capillarity, inertia, and viscous force arising from the air entrainment between the drop and the substrate, which makes this work fundamentally distinct from the case of the

stationary and hydrophilic surfaces [18,21]. The most surprising feature is, compared with its stationary counterpart, a 40% reduction of the contact time is easily attainable by just exerting a horizontal motion of the surface of a few m/s [Fig. 3(c)], which is expected to be a strategy to realize rapid water repellency. We expect that our findings would be applicable for other types of situations when relative horizontal motion happens between the drop and the surface. It would be interesting to extend our results to the case of Leidenfrost drops or viscous liquids. These insights could help develop novel strategies for controlling drop impact dynamics [35], which will shed new light on practical applications.

This work received financial support from the National Natural Science Foundation of China (Grants No. 52075071, No. 51605073, No. 11872227, No. 11632009) and Hong Kong Research Grants Council (Grant No. 11219219).

*Corresponding author.
cunjinglv@mail.tsinghua.edu.cn
†Corresponding author.
yahualiu@dlut.edu.cn

[1] D. Richard, C. Clanet, and D. Quéré, Nature (London) **417**, 811 (2002).
[2] Y. Liu, L. Moevius, X. Xu, T. Qian, J. M. Yeomans, and Z. Wang, Nat. Phys. **10**, 515 (2014).
[3] A. M. Moqaddam, S. S. Chikatamarla, and I. Karlin, J. Fluid Mech. **824**, 866 (2017).
[4] T. M. Schutzius, S. Jung, T. Maitra, G. Graeber, M. Kohme, and D. Poulikakos, Nature (London) **527**, 82 (2015).
[5] H.-J. Butt, I. V. Roisman, M. Brinkmann, P. Papadopoulos, D. Vollmer, and C. Semprebon, Curr. Opin. Colloid Interface Sci. **19**, 343 (2014).
[6] T. L. Liu and C.-J. C. Kim, Science **346**, 1096 (2014).
[7] L. Mishchenko, B. Hatton, V. Bahadur, J. A. Taylor, T. Krupenkin, and J. Aizenberg, ACS Nano **4**, 7699 (2010).
[8] D. Wang, Q. Sun, M. J. Hokkanen, C. Zhang, F.-Y. Lin, Q. Liu, S.-P. Zhu, T. Zhou, Q. Chang, B. He, Q. Zhou, L. Chen, Z. Wang, H. A. R. Ras, and X. Deng, Nature (London) **582**, 55 (2020).
[9] N. Miljkovic, R. Enright, Y. Nam, K. Lopez, N. Dou, J. Sack, and E. N. Wang, Nano Lett. **13**, 179 (2013).
[10] H. A. Stone, ACS Nano **6**, 6536 (2012).
[11] P.-B. Bintein, H. Lhuissier, A. Mongruel, L. Royon, and D. Beysens, Phys. Rev. Lett. **122**, 098005 (2019).
[12] S.-H. Lee, K. Harth, M. Rump, M. Kim, D. Lohse, K. Fezzaa, and J. H. Je, Soft Matter **16**, 7935 (2020).
[13] J. C. Bird, R. Dhiman, H.-M. Kwon, and K. K. Varanasi, Nature (London) **503**, 385 (2013).
[14] P. Chantelot, A. M. Moqaddam, A. Gauthier, S. S. Chikatamarla, C. Clanet, I. V. Karlin, and D. Quéré, Soft Matter **14**, 2227 (2018).
[15] L. Wang, R. Wang, J. Wang, and T.-S. Wong, Sci. Adv. **6**, eabb2307 (2020).
[16] M. Song, Z. Liu, Y. Ma, Z. Dong, Y. Wang, and L. Jiang, NPG Asia Mater. **9**, e415 (2017).
[17] O. A. Povarov, O. I. Nazarov, L. A. Ignatevskaya, and A. I. Nikolskii, J. Eng. Phys. **31**, 1453 (1976).
[18] H. Almohammadi and A. Amirfazli, Soft Matter **13**, 2040 (2017).
[19] X. Zhang, Z. Zhu, C. Zhang, and C. Yang, Appl. Phys. Lett. **117**, 151602 (2020).
[20] S. Buksh, M. Marengo, and A. Amirfazli, Atom. Sprays **30**, 557 (2020).
[21] H. Almohammadi and A. Amirfazli, Langmuir **33**, 5957 (2017).
[22] See Supplemental Material at http://link.aps.org/supplemental/10.1103/PhysRevLett.126.234503 for additional experimental details, supplemental figures (Figs. S1–S6), and movies (Movies S1–S3).
[23] L. D. Landau and E. M. Lifschitz, *Course of Theoretical Physics*, Vol. 2, 2nd ed. (Pergamon Press, Oxford, 1987).
[24] C. Josserand and S. T. Thoroddsen, Annu. Rev. Fluid Mech. **48**, 365 (2016).
[25] C. Clanet, C. Béguin, D. Richard, and D. Quéré, J. Fluid Mech. **517**, 199 (2004).
[26] A. Gauthier, S. Symon, C. Clanet, and D. Quéré, Nat. Commun. **6**, 8001 (2015).
[27] M. Reyssat, D. Richard, C. Clanet, and D. Quéré, Faraday Discuss. **146**, 19 (2010).
[28] C.-H. Choi and C.-J. Kim, Phys. Rev. Lett. **96**, 066001 (2006).
[29] J. de Ruiter, R. Lagraauw, D. van den Ende, and F. Mugele, Nat. Phys. **11**, 48 (2015).
[30] T. Tran, H. J. J. Staat, A. Susarrey-Arce, T. C. Foertsch, A. van Houselt, H. J. G. E. Gardeniers, A. Prosperetti, D. Lohse, and C. Sun, Soft Matter **9**, 3272 (2013).
[31] J. Hao, J. Lu, L. Lee, Z. Wu, G. Hu, and J. M. Floryan, Phys. Rev. Lett. **122**, 054501 (2019).
[32] G. Riboux and J. M. Gordillo, Phys. Rev. Lett. **113**, 024507 (2014).
[33] A. Gauthier, J. C. Bird, C. Clanet, and D. Quéré, Phys. Rev. Fluids **1**, 084002 (2016).
[34] C. Duez, C. Ybert, C. Clanet, and L. Bocquet, Nat. Phys. **3**, 180 (2007).
[35] A. L. Yarin, Annu. Rev. Fluid Mech. **38**, 159 (2006).